

The broad O VI absorber at $z = 3.02$ toward CTQ 325*

S. A. Levshakov¹, S. D’Odorico², I. I. Agafonova¹, and M. Dessauges-Zavadsky³

¹ Department of Theoretical Astrophysics, Ioffe Physico-Technical Institute, 194021 St.Petersburg, Russia

² European Southern Observatory, Karl-Schwarzschild-Strasse 2, D-85748 Garching bei München, Germany

³ Observatoire de Genève, CH-1290 Sauverny, Switzerland

Received 00 / Accepted 00

Abstract. We report on the multiphase absorption-line system detected at a redshift $z_{\text{abs}} = 3.021$ in the spectrum of the quasi-stellar object CTQ 325 ($z_{\text{em}} = 3.212$). The system is displaced by $\simeq 14,000 \text{ km s}^{-1}$ to the blue of the systemic velocity defined by the center of the symmetric O I quasar emission line. It consists of shallow and broad ($\sim 700 \text{ km s}^{-1}$ FWHM) absorption lines of H I $\lambda 1215$, C IV $\lambda\lambda 1548, 1550$, and O VI $\lambda\lambda 1032, 1038$, produced by collisionally ionized gas and of narrow absorption lines (FWHM $< 20 \text{ km s}^{-1}$) of Ly $\alpha_{\alpha,\beta,\dots,6}$, Si III $\lambda 1206$, and C III $\lambda 977$ produced by photoionized gas. Possible origins of this system are discussed.

Key words. Cosmology: observations – Line: formation – Line: profiles – Galaxies: abundances – Quasars: absorption lines – Quasars: individual: CTQ 325

1. Introduction

While performing a study of the high-resolution spectrum of the distant quasar CTQ 325 from the Calán-Tololo Survey (Maza et al. 1996), we experienced problems in the continuum placement and the subsequent analysis of the normalized data for the regions $\lambda\lambda = 4100\text{--}4200 \text{ \AA}$, $4850\text{--}4950 \text{ \AA}$ and $6200\text{--}6280 \text{ \AA}$. The original spectrum, shown in Fig. 1, exhibits bumps and shallow troughs in these regions which could hardly be expected from the QSO continuum itself. Can these irregularities be attributed to shallow broad absorption lines or are they artifacts resulting from inappropriate data reduction?

Calibration flux errors can be excluded in our case since these features are present in all three unnormalized spectra we have for this range of exposure time of 4100s each. The broad features are located in the middle of echelle orders, so they cannot be explained by a bad merging of the orders as well. The spectrum of other quasar CTQ 298 taken during the same set of observations with the UVES/VLT does not show any peculiarities in these spectral ranges. In a composite QSO spectrum (Telfer et al. 2002) there are no weak emission-line features which could mimic bumps and troughs in the Ly α forest similar to that observed in CTQ 325. Thus we conclude that the broad absorption features we see in CTQ 325 are real.

The identification of these lines is straightforward: if the broad absorption at $\lambda \simeq 6225\text{--}6230 \text{ \AA}$ is the unre-

solved doublet C IV $\lambda\lambda 1548, 1551$ at $z_{\text{abs}} = 3.021$, then the absorptions at $\lambda \simeq 4172, 4149$, and 4888 \AA are, respectively, O VI $\lambda 1032$, O VI $\lambda 1038$, and Ly α (the expected positions of N V $\lambda\lambda 1238, 1242$ are blended with the blue wing of the damped Ly α at $z_{\text{abs}} = 3.118$).

Similar shallow (the central optical depth $\tau_0 < 1$) broad (FWHM $> 100 \text{ km s}^{-1}$) absorption line systems can be found in other QSOs. For example, in the spectrum of PG 2302+029 ($z_{\text{em}} = 1.052$) a very broad (FWHM $> 3000 \text{ km s}^{-1}$) absorption complex consisting of unresolved doublets of C IV, N V, and O VI (Ly α is undetectable) was found at a redshift ~ 0.695 that corresponds to the blueshifted ‘ejection’ velocity of $\sim 56,000 \text{ km s}^{-1}$ (Jannuzi et al. 1996). A weak C IV trough with FWHM $\sim 800 \text{ km s}^{-1}$ at the blueshifted velocity $\sim 4000 \text{ km s}^{-1}$ ($z_{\text{abs}} = 4.045$) is present in the spectrum of FIRST 0747+2739 — a quasar with a redshift of 4.11 (Richards et al. 2002). Besides, in the published spectrum the shallow and broad absorption features at the expected positions of the Ly α and N V $\lambda 1242$ lines can be found as well (see Fig. 1 in Richards et al.). An absorption system at $z = 2.146$ with broad and shallow C IV and N V doublets (FWHM $\gtrsim 1000 \text{ km s}^{-1}$) and weak Ly α was identified in the spectrum of Tol 1038–2712 ($z_{\text{em}} = 2.331$) which belongs to the famous ‘Tololo pair’ (e.g., Dinshaw & Impey 1996; Srianand & Petitjean 2001).

The interpretation of these shallow and broad systems is not unique. Highly ionized gas can reside inside the quasar host galaxy, be ejected from the galaxy, or trace the intergalactic medium (IGM). For instance, the absorber in PG 2302+029 is intrinsic since the comparison of spectra

Send offprint requests to: S. A. Levshakov

* Based on observations obtained at the VLT Kueyen telescope (ESO, Paranal, Chile), the ESO programme 69.A-0123.

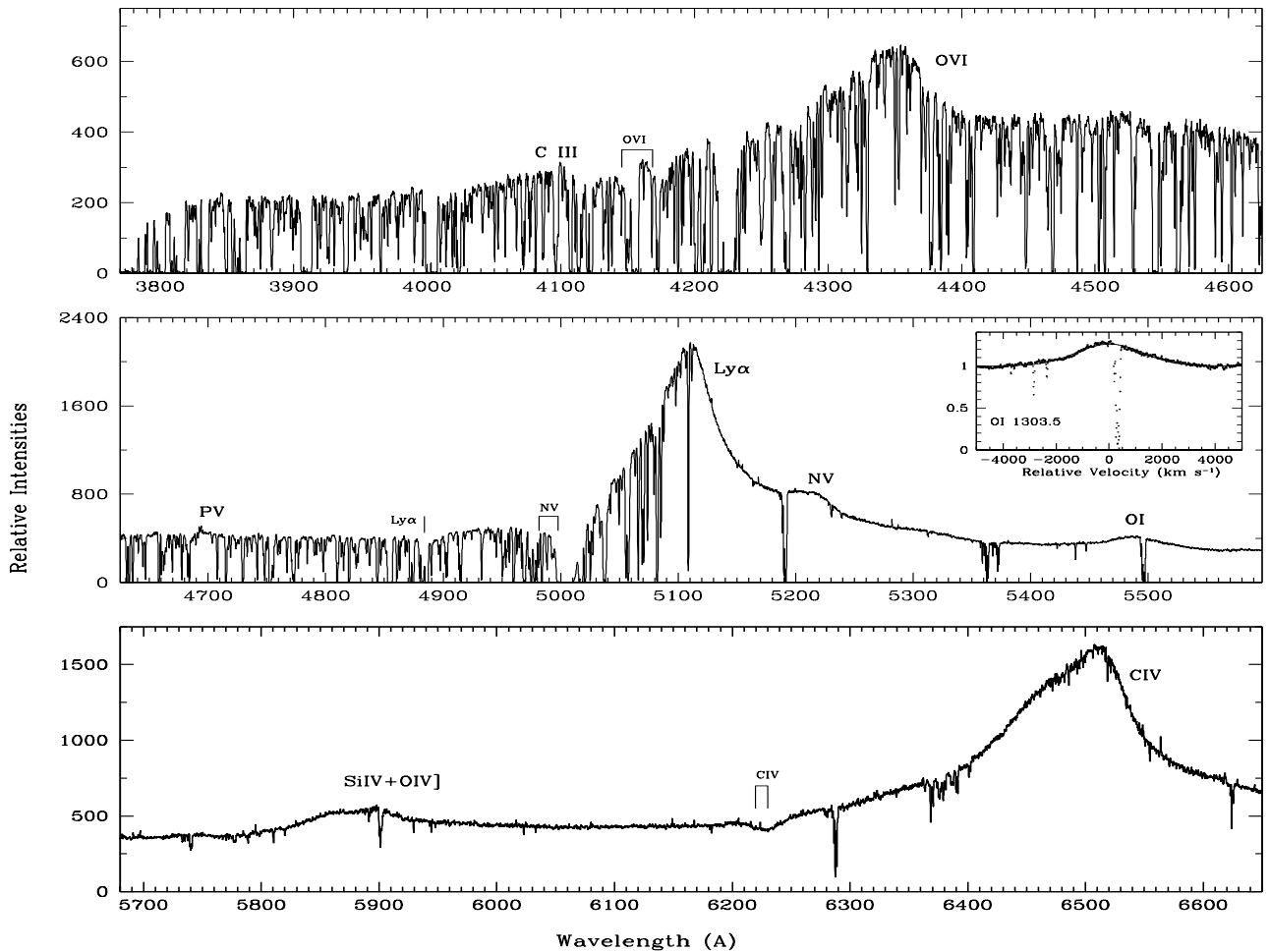


Fig. 1. VLT/UVES spectra of CTQ 325 as a function of vacuum heliocentric wavelength. The spectral resolution is $\simeq 6.5 \text{ km s}^{-1}$ (FWHM). The identification of the emission lines are indicated near each spectrum. A smooth fit by a Gaussian (solid curve) to the normalized O I $\lambda 1303.5$ emission profile (dots), shown in the inset in the middle panel, provides the QSO redshift $z_{\text{em}} = 3.21196 \pm 0.00010$ (2σ). The peaks of the asymmetric Ly α , C IV $\lambda 1549.1$ and a weak P V $\lambda 1118$ emission lines are blueshifted by $\sim 570 \text{ km s}^{-1}$ with respect to this O I line giving $z'_{\text{em}} = 3.20$ in agreement with low-resolution observations by Lopez et al. (2001). Vertical marks indicate the broad absorption lines at $z_{\text{abs}} = 3.0212$.

taken for this QSO in 1994 and 1998 revealed that ‘O VI and N V dramatically weakened to become unmeasurable’ (Sabra et al. 2003). On the other hand, the above mentioned Tololo absorber is probably an example of the intervening system (a putative supercluster or filament) since a damped Ly α system [$\log N(\text{H I}) \sim 19.7$, from Srianand & Petitjean 2001] at the same redshift $z = 2.14$ is seen in the companion quasar Tol 1037–2704 ($z_{\text{em}} = 2.207$) separated by $\sim 4 \text{ Mpc}$ from the line of sight toward Tol 1038–2712. In general, the interpretation of quasar absorption-line systems is not such straightforward and requires accounting for all available data.

In this paper, we present the quantitative analysis of the $z_{\text{abs}} = 3.0212$ system toward CTQ 325. Possible explanations of its nature are discussed in Sect. 4.

2. Observations

The quasar CTQ 325 ($\alpha = 13^{\text{h}}42^{\text{m}}58.9^{\text{s}}$, $\delta = -13^{\circ}55'59.9''$, J2000; $m_B = 18.3$; Lopez et al. 2001) was observed with the VLT/UVES over the nights 16–18 March, 2002. The spectrum covers the range between 3750 and 9900 Å, with wavelength gaps between 5597–5677 Å and 7940–8077 Å. The resulting spectral resolution is between 6.3 and 6.8 km s^{-1} FWHM, and the S/N ratio per pixel $\simeq 40$ –50 ($\lambda \simeq 3800$ –4700 Å) and $\text{S/N} > 50$ ($\lambda \simeq 4700$ –6600 Å). The data reduction was performed using the ECHELLE context routines implemented in the ESO MIDAS package. The details of the reduction procedure is outlined in Molaro et al. (2000). The uncertainties in the continuum placement are not larger than 5% due to high S/N and high spectral resolution.

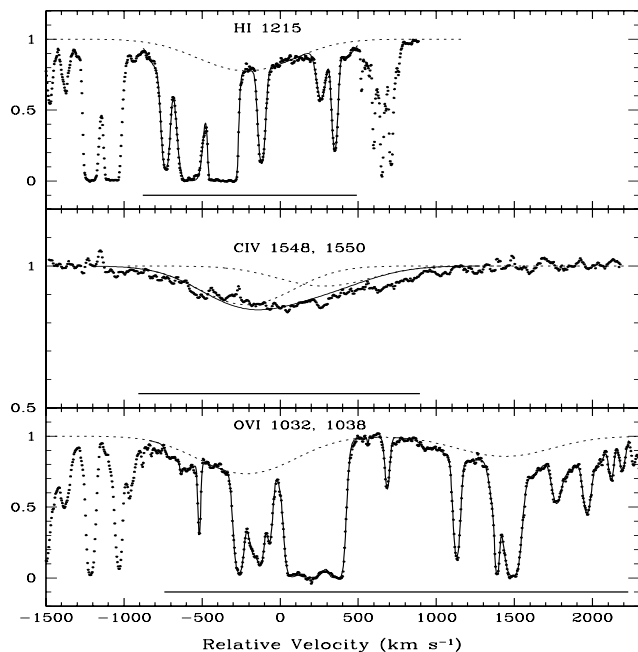


Fig. 2. Observed absorption lines in the spectrum of CTQ 325 (dots) and over-plotted synthetic profiles (solid curves) calculated from the joint analysis of the shallow broad and narrow components. The zero radial velocity is fixed at $z_{\text{abs}} = 3.0212$. Bold horizontal lines mark pixels included in the optimization procedure. In addition, synthetic profiles of broad Ly α , C IV $\lambda\lambda 1548, 1550$, and O VI $\lambda\lambda 1032, 1038$ are shown separately (dashed curves). For each doublet, the velocity scale refers to the first component.

3. Analysis

Emission-line redshift. One of the noticeable features of the spectrum of CTQ 325 is that the blue side wing of the C IV emission line, which is not affected by numerous absorption lines, has a longer tail than the redward side (Fig. 1). This blue-side asymmetry is also seen in the profiles of Ly α and O VI, whereas the neutral oxygen line O I $\lambda 1303.5$ is symmetric, providing us with the accurate measurement of the emission redshift of the QSO, $z_{\text{em}} = 3.21196 \pm 0.00010$ (2σ).

From earlier studies (e.g., Gaskell 1982; Espey et al. 1989; Tytler & Fan 1992) it was found that the mean blueshift of Ly α , C IV, and NV with respect to O I and Mg II is about 600 km s^{-1} . The same order of magnitude blueshift of $\sim 570 \text{ km s}^{-1}$ was measured in our case between the center of the O I line and the peaks of the Ly α , C IV, and P V lines. This could indicate that the redshift of CTQ 325 is slightly higher than $z'_{\text{em}} = 3.20$ previously deduced from low-resolution data (FWHM = 5.2 \AA) by Lopez et al. (2001).

The O VI absorber at $z_{\text{abs}} = 3.0212$. The analysis of the broad complex is illustrated in Fig. 2. We found that all lines can be well fitted by a simple Gaussian with the broadening b -parameter of $412 \pm 20 \text{ km s}^{-1}$, and column

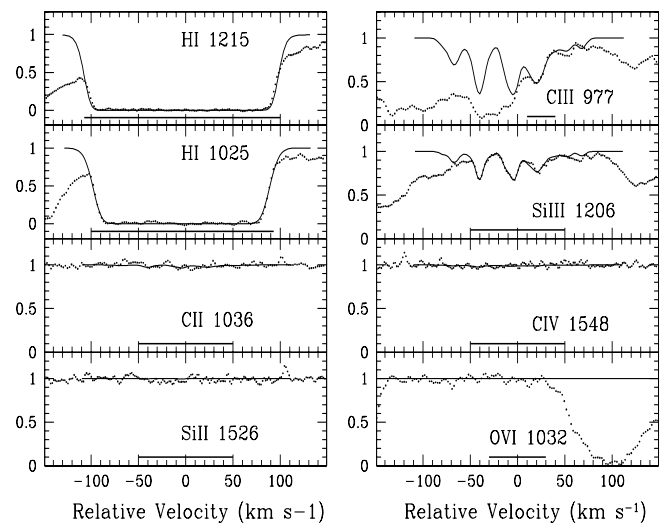


Fig. 3. Hydrogen and metal lines associated with the $z_{\text{abs}} = 3.0192$ low-ionized absorber toward CTQ 325 (dots). Smooth lines are the synthetic spectra convolved with the corresponding point-spread functions. Bold horizontal lines mark pixels included in the MCI procedure. Continuum windows at the positions of C II $\lambda 1036$, Si II $\lambda 1526$, C IV $\lambda 1548$, and O VI $\lambda 1032$ are shown as well. The normalized $\chi^2_{\text{min}} = 0.92$ (the number of degrees of freedom $\nu = 400$).

densities $N(\text{H I}) = (1.38 \pm 0.07) \times 10^{14} \text{ cm}^{-2}$, $N(\text{C IV}) = (1.37 \pm 0.07) \times 10^{14} \text{ cm}^{-2}$, and $N(\text{O VI}) = (6.2 \pm 0.3) \times 10^{14} \text{ cm}^{-2}$. Since the shallow profiles of the Ly α and O VI lines are affected by the narrow forest lines, we included in the fitting procedure the whole regions marked in Fig. 2 by the bold horizontal lines. All three regions with the broad H I $\lambda 1215$, C IV $\lambda\lambda 1548, 1550$, and O VI $\lambda\lambda 1032, 1038$ were analyzed simultaneously. The corresponding equivalent widths are as follows (rest frame values): $W_{\lambda}(\text{H I}_{1215}) \simeq 190 \text{ m\AA}$, $W_{\lambda}(\text{C IV}_{1548+1550}) \simeq 210 \text{ m\AA}$, $W_{\lambda}(\text{O VI}_{1032}) \simeq 190 \text{ m\AA}$, and $W_{\lambda}(\text{O VI}_{1038}) \simeq 95 \text{ m\AA}$, and the central optical depths are $\tau_0 = 0.25, 0.15, 0.31$, and 0.15 , respectively.

The estimated column density ratios $N(\text{C IV})/N(\text{H I}) \sim 1$ and $N(\text{O VI})/N(\text{H I}) \sim 4.5$ indicate that the gas is collisionally ionized and the kinetic temperature $\log T > 5$ (see Figs. 1 and 2 in Levshakov et al. 2003a). If we assume that the metallicity pattern is solar, then according to Sutherland & Dopita (1993) the optimal value for the kinetic temperature is $\log T = 5.30$. At this temperature we find the total column densities of hydrogen, carbon, and oxygen being $N(\text{H}) \simeq 4.3 \times 10^{19} \text{ cm}^{-2}$, $N(\text{C}) \simeq 1.2 \times 10^{16} \text{ cm}^{-2}$, and $N(\text{O}) \simeq 3.0 \times 10^{16} \text{ cm}^{-2}$, i.e. the metal content in this absorber is slightly over solar, $[\text{C}/\text{H}] \simeq 0.05$ and $[\text{O}/\text{H}] \simeq 0.15$ ¹.

¹ $[\text{X}/\text{Y}] \equiv \log(\text{X}/\text{Y}) - \log(\text{X}/\text{Y})_{\odot}$. Throughout the text photospheric solar abundances for C and O are taken from Allende Prieto et al. (2001, 2002), and for Si from Holweger (2001).

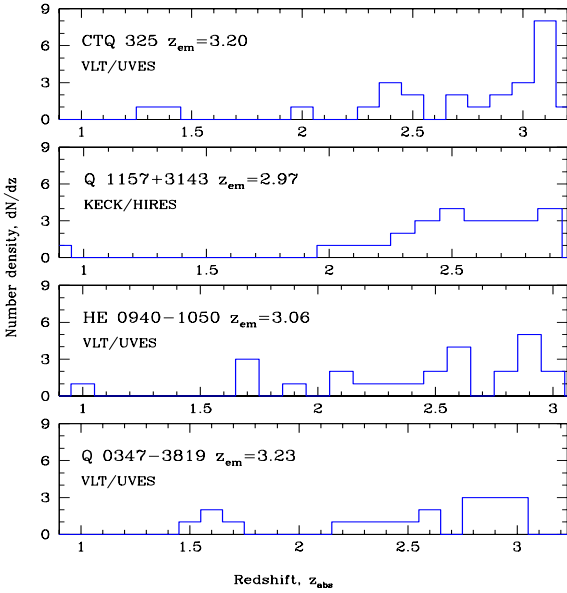


Fig. 4. Number density distributions of metal absorbers toward CTQ 325 (this paper), Q 1157+3143 and HE 0940–1050 (Levshakov et al. 2003c), and Q 0347–3819 (Levshakov et al. 2002b). QSO spectra with similar quality observations are used. The adopted bin size is $\Delta z = 0.1$.

The narrow absorption lines beneath the broad Ly α in Fig. 2 at $\Delta v \simeq -519, -365, -150,$ and 95 km s^{-1} are the Ly α lines which have corresponding Ly β and higher order Lyman series lines up to Ly $_6$. The strongest of these absorbers, that at $\Delta v \simeq -150 \text{ km s}^{-1}$, shows metal absorption in the Si III $\lambda 1206$ and partially blended C III $\lambda 977$ lines and line-free continuum at the expected positions of the C II $\lambda 1334$, Si II $\lambda 1526$, C IV $\lambda 1548$, and O VI $\lambda 1032$ lines (Fig. 3).

We have analyzed this metal system with the Monte Carlo Inversion (MCI) procedure (Levshakov et al. 2000, 2002a) with three different UV ionizing backgrounds: the power law $J_\nu \propto \nu^{-1.5}$, the Mathews-Ferland spectrum (Mathews & Ferland 1987, hereafter MF), and the Haardt-Madau spectrum (Haardt & Madau 1996, hereafter HM). Since hydrogen lines in this system are saturated, we were able to estimate only the lower limit of $N(\text{H I}) \gtrsim 2 \times 10^{16} \text{ cm}^{-2}$. Analyzing simultaneously all available metal lines (including those presented only as upper limits), we obtained the mean ionization parameter $U_0 \simeq 1.3 \times 10^{-3}$, total hydrogen column density $N(\text{H}) \gtrsim 10^{18} \text{ cm}^{-2}$ and metal content $[\text{C}/\text{H}] \lesssim -1.0$, $[\text{Si}/\text{H}] \lesssim -0.9$ for the MF and $\nu^{-1.5}$ spectra, and $U_0 \simeq 2.4 \times 10^{-3}$, $N(\text{H}) \gtrsim 5 \times 10^{18} \text{ cm}^{-2}$ and $[\text{C}/\text{H}] \lesssim -1.5$, $[\text{Si}/\text{H}] \lesssim -1.5$ for the HM spectrum. The estimated column densities for particular ions are as follows: $N(\text{C II}) < 6.0 \times 10^{12} \text{ cm}^{-2}$, $N(\text{Si II}) < 6.0 \times 10^{11} \text{ cm}^{-2}$, $N(\text{Si III}) = (3.5 \pm 0.4) \times 10^{12} \text{ cm}^{-2}$, $N(\text{C III}) \sim 3 \times 10^{13} \text{ cm}^{-2}$ (uncertain because of blending), and $N(\text{C IV}) < 2.0 \times 10^{12} \text{ cm}^{-2}$.

Taking the metagalactic value of the mean specific intensity at the hydrogen Lyman edge $J_{912}(z=3) = 0.4 \times 10^{-21} \text{ ergs cm}^{-2} \text{ s}^{-1} \text{ Hz}^{-1} \text{ sr}^{-1}$ from HM, we calculate

Table 1. Metal absorbers toward CTQ 325

z_{abs}	Species identified
1.3975	Mg II _{2796,2803} , Al III _{1854,1862}
1.4031	Mg II _{2796,2803} , Al II ₁₆₇₀ , Al III _{1854,1862}
2.0902	C IV _{1548,1550}
2.3785	Ly α , C IV _{1548,1550}
2.4315	Ly α , Si III ₁₂₀₆ , C IV _{1548,1550} , Si IV ₁₃₉₃
2.4615	Ly α , C IV _{1548,1550}
2.4775	Ly α , Si III ₁₂₀₆ , C IV ₁₅₅₀
2.5025	Ly α , C IV _{1548,1550}
2.5126	Ly α , C IV _{1548,1550}
2.7392	Ly α, β , C IV _{1548,1550}
2.7531	Ly α, β , C IV _{1548,1550}
2.8903	Ly α, β, γ , C IV _{1548,1550}
2.9098	Ly α, β , O VI ₁₀₃₁
2.9933	Ly α, β, γ , C IV _{1548,1550}
3.0096	Ly $\alpha, \beta, \gamma, \delta$, C III ₉₇₇ , C IV ₁₅₄₈
3.0212	Ly α , C IV _{1548,1550} , O VI _{1031,1037}
3.0680	Ly α , C IV _{1548,1550}
3.1136	Ly $\alpha, \dots, 10$, C III ₉₇₇ , C IV _{1548,1550} , N V ₁₂₃₈ , O VI ₁₀₃₁
3.1148	Ly $\alpha, \dots, 9$, C III ₉₇₇ , Si III ₁₂₀₆ , C IV _{1548,1550} , Si IV _{1393,1402} , O VI ₁₀₃₁
3.1184	Ly $\alpha, \dots, 10$, N I _{1199.5,1200.2} , O I _{950,976,988,1039,1302} , Ar I ₁₀₄₈ , C II _{1036,1334} , N II ₁₀₈₃ , Mg II ₁₂₃₉ , Al II ₁₆₇₀ , Si II _{989,1020,1190,1193,1260,1304,1526,1808} , P II _{963,1152} , P III ₁₃₀₁ , S II _{1250,1253,1259} , Fe II _{940,1063,1081,1096,1608} , Ni II _{1317,1454,1741} , C III ₉₇₇ , Si III ₁₂₀₆ , C IV _{1548,1550}
3.1274	Ly $\alpha, \dots, 7$, C III ₉₇₇ , C IV _{1548,1550} , O VI ₁₀₃₁
3.1284	Ly $\alpha, \dots, 7$, C III ₉₇₇ , C IV _{1548,1550} , Si IV ₁₃₉₃ , N V ₁₂₃₈ , O VI ₁₀₃₁
3.1438	Ly $\alpha, \beta, \gamma, \delta$, C IV ₁₅₄₈ , O VI ₁₀₃₇
3.1701	Ly α, β , O VI ₁₀₃₁
3.1711	Ly α, β, γ , O VI ₁₀₃₁
3.2024	Ly α, β , N V ₁₂₃₈ , O VI _{1031,1037}

the mean number density $n_0 \simeq 3.5 \times 10^{-2} \text{ cm}^{-3}$ and the linear size $L \gtrsim 10 \text{ pc}$ (MF and $\nu^{-1.5}$), and $n_0 \simeq 10^{-2} \text{ cm}^{-3}$, $L \gtrsim 150 \text{ pc}$ (HM). The mean kinetic temperature is estimated as $(1.5 - 2) \times 10^4 \text{ K}$. From the non-detection of C II and Si II lines we can also deduce the upper limit of $N(\text{H I}) < 10^{18} \text{ cm}^{-2}$, since otherwise the self-shielding, important at $N(\text{H I}) > 3 \times 10^{17} \text{ cm}^{-2}$, would shift the ionization state toward these low-ionization transitions. Thus, in any case the size of the absorber at $\Delta v = -150 \text{ km s}^{-1}$ is not larger than 1 kpc. The gas density will be substantially higher and the linear size smaller if the absorber is located close to the QSO where the intensity of the local ionizing background is enhanced by the direct QSO radiation.

Unfortunately, other narrow Ly α -line absorbers have blends at the expected positions of metals which makes impossible any quantitative conclusions about their physics.

4. Discussion

Equipped with the results obtained in the previous section we can now consider the possible causes for the observed absorptions.

The narrow line system is probably physically connected with the shallow absorber since both the detected ions (Si III and C III) and the linear size ($L \sim 100$ pc) are very unusual for a ‘stand alone’ intervening system: most QSO absorbers exhibit C IV lines and have linear sizes of $L \sim 10$ kpc. Thus what we observe is a metal-poor cool and photoionized cloud(s) embedded in hot collisionally ionized gas with solar metal content. Most plausible origin of this structure can provide the jet-cloud interaction – the phenomenon well known from the radio observations of active galactic nuclei (e.g., Carvalho & O’Dea 2002 and references therein). In this scenario, the shock (blast) wave driven by the QSO jet strikes an intervening cloud embedded in the interstellar medium. Model calculations and model experiments of shock-cloud interaction (Klein et al. 1994; Klein et al. 2003) show that this process leads to the cloud fragmentation and produces the velocity dispersion of $\sim 0.1v_{\text{blast}}$. After fragmentation, the cloud material continues to be accelerated until it is approximately comoving with the surrounding gas in the jet. In addition, shock compresses the cloud gas which can enhance its cooling rate. It is to be noted that typical parameters of the AGN jets are: radius ~ 500 pc, length-to-radius ratio $\sim 100 : 1$, and expansion velocity ~ 1000 km s $^{-1}$ (Carvalho & O’Dea 2002).

Difference in metallicities between the collisionally ionized gas and gas in the narrow-line absorber can also be explained within the frame of the jet-cloud interaction. Namely, solar and oversolar metallicities are characteristic for the QSO circumnuclear gas (e.g., Hamann & Ferland 1999), whereas the metallicity of the ambient interstellar matter is much lower ($Z < 0.1Z_{\odot}$).

The profiles of the QSO emission lines Ly α , C IV, and O VI are highly asymmetric indicating strong outflows. The shallow and broad absorber is blueshifted by $\sim 14,000$ km s $^{-1}$ from the systemic velocity (defined by the center of the symmetric O I quasar emission line) and lies at the high ejection end of the asymmetric emission lines. Whether this is a chance coincidence or the absorber is indeed located very close to the QSO emission line region can be tested in monitoring this quasar over the course of a few years: variability of the absorption profiles would testify the internal origin. Sometimes the close location of the absorption system leads to incomplete coverage of the central light source. This results in flat line profiles not going to zero intensities and/or in unexpected doublet ratios. None of these features is observed in the present absorption systems.

Another evidence of the high activity of CTQ 325 can be found from the distribution of metal absorbers along the line of sight (see Table 1). Thus, Fig. 4 shows that in the range $3.0 \lesssim z \lesssim 3.1$ the number density dN/dz exceeds essentially the mean value. However, this argument

is not unambiguous since one cannot exclude the observed overdensity as being due to the clustering of the intervening absorbers (e.g., in Fig. 4, the region $z > 2.7$ toward Q 1157+3143 was considered as a possible supercluster by Ganguly et al. 2001).

Although the jet-cloud origin is consistent with all recovered parameters of this broad-hot + narrow-cool absorption system, another interpretation — absorption by warm gas in the intervening large scale structure (LLS) object — is also possible (motivated mostly by the Tololo pair). In this case the collisionally ionized phase may be produced by shocks driven by the accretion of gas into the potential well. If typical size of a putative cluster is $R \sim 1$ Mpc, then the velocity dispersion of the warm gas component of ~ 400 km s $^{-1}$ gives the total mass $M_{\text{cl}} \sim 2 \times 10^{13} M_{\odot}$. High metallicity estimated for the collisionally ionized gas is in line with that usually measured in clusters of galaxies (e.g., Rosati et al. 2002). The presence of the compact cool absorbers may also be expected: the ionic composition of our narrow line absorber at $v \simeq -150$ km s $^{-1}$ is very much alike to that observed in a cloud in the Virgo supercluster, (see Fig. 2 in Tripp et al. 2002). The size of this cloud was estimated as 70 pc only. The existence of massive megaparsec-scale structures at high redshift (from $z = 2.16$ up to $z = 4.10$) has recently been confirmed by direct observations of distant (proto) clusters (Venemans et al. 2002, 2003).

5. Conclusions

We show that the shallow and broad C IV, O VI, and Ly α lines detected at $z_{\text{abs}} = 3.021$ in the spectrum of CTQ 325 are produced by *collisionally* ionized gas. The narrow line absorber detected at the same redshift reveals the ionization state expected for a cool photoionized medium — strong saturated hydrogen lines, absorptions in C III and Si III, and no high ionization lines like C IV or O VI. Collisionally ionized gas has the near solar metallicity, whereas the metal content of the photoionized component is less than $0.1Z_{\odot}$.

The observed multiphase structure can be well described in the framework of the jet-cloud interaction. However, the absorption by the shocked accreting gas in the intervening LSS object cannot be excluded. At the moment there are no unambiguous tests to select between these possibilities.

Acknowledgements. The work of S.A.L. and I.I.A. is partly supported by the RFBR grant No. 03-02-17522.

References

- Allende Prieto, C., Lambert, D. L., & Asplund, M. 2001, ApJ, 556, L63
- Allende Prieto, C., Lambert, D. L., & Asplund, M. 2002, ApJ, 573, L137
- Carvalho, J. C., & O’Dea, C. P. 2002, ApJS, 141, 337
- Dinshaw, N., & Impey, C. D. 1996, ApJ, 458, 73

- Espey, B. R., Carswell, R. F., Bailey, J. A., Smith, M. G., & Ward, M. 1989, *ApJ*, 342, 666
- Gaskell, C. M. 1982, *ApJ*, 263, 79
- Ganguly, R., Charlton, J. C., & Bond, N. A. 2001, *ApJ*, 553, L101
- Haardt, F., & Madau, P. 1996, *ApJ*, 461, 20 [HM]
- Hamann, F., & Ferland, G. 1999, *ARA&A*, 37, 487
- Holweger, H. 2001, in *Solar and Galactic Composition*, ed. R. F. Wimmer-Schweingruber, *AIP Conf. Proc.*, 598, 23
- Jannuzi, B. T., Hartig, G. F., Kirhakos, S. et al. 1996, *ApJ*, 470, L11
- Klein, R. I., McKee, C. F., & Colella, P. 1994, *ApJ*, 420, 213
- Klein, R. I., Budil, K. S., Perry, T. S., & Bach, D. P. 2003, *ApJ*, 583, 245
- Levshakov, S. A., Agafonova, I. I., Reimers, D., & Baade, R. 2003a, *A&A*, 404, 449
- Levshakov, S. A., Agafonova, I. I., D'Odorico, S., Wolfe, A. M., & Dessauges-Zavadsky, M. 2003b, *ApJ*, 582, 596
- Levshakov, S. A., Agafonova, I. I., Molaro, P., Centurión, M., & Tytler, D. 2003c, *A&A*, submitted
- Levshakov, S. A., Agafonova, I. I., Centurión, M., & Mazets, I. E. 2002a, *A&A*, 383, 813
- Levshakov, S. A., Dessauges-Zavadsky, M., D'Odorico, S., & Molaro, P. 2002b, *ApJ*, 565, 696
- Levshakov, S. A., Agafonova, I. I., & Kegel, W. H. 2000, *A&A*, 360, 833
- Lopez, S., Maza, J., Masegosa, J., & Marquez, I. 2001, *A&A*, 366, 387
- Mathews, W. G., & Ferland, G. J. 1987, *ApJ*, 323, 456 [MF]
- Maza, J., Wischnjewsky, M., & Antezana, R. 1996, *RMxA&A*, 32, 35
- Molaro, P., Bonifacio, P., Centurión, M. et al. 2000, *ApJ*, 541, 54
- Richards, G. T., Gregg, M. D., Becker, R. H., & White, R. L. 2002, *ApJ*, 567, L13
- Rosati, P., Borgani, S., & Norman, C. 2002, *ARA&A*, 40, 539
- Sabra, B. M., Hamann, F., Jannuzi, B. T., George, I. M., & Shields, J. C. 2003, *ApJ*, 590, 66
- Srianand, R., & Petitjean, P. 2001, *A&A*, 373, 816
- Sutherland, R. S., & Dopita, M. A. 1993, *ApJS*, 88, 253
- Telfer, R. C., Zheng, W., Kriss, G. A., & Davidsen, A. F. 2002, *ApJ*, 565, 773
- Tripp, T. M., Jenkins, E. B., Williger, G. M. et al. 2002, *ApJ*, 575, 697
- Tytler, D., & Fan, X.-M. 1992, *ApJS*, 79, 1
- Venemans, B., Miley, G., Kurk, J., Röttgering, H., & Pentericci, L. 2003, *Messenger*, 111, 36
- Venemans, B. P., Kurk, J. D., Miley, G. K. et al. 2002, *ApJ*, 569, L1